Particuology 40 (2018) 1–9

Contents lists available at ScienceDirect

Particuology

journal homepage: www.elsevier.com/locate/partic

Frequency–amplitude behavior in the incipient movement of grains under vibration

Karina A. Valenzuela Aracena[a], Jesica G. Benito[a], Luc Oger[b], Irene Ippolito[c], Rodolfo O. Uñac[a], Ana M. Vidales[a,*]

[a] INFAP, CONICET, Departamento de Física, Facultad de Ciencias Físico Matemáticas y Naturales, Universidad Nacional de San Luis, Ejército de los Andes 950, D5700HHW, San Luis, Argentina
[b] Institut de Physique de Rennes, UMR UR1-CNRS 6251, Université de Rennes 1, 263, Avenue du Général Leclerc, Campus de Beaulieu, CS 74205, 35042 Rennes Cedex, France
[c] Universidad de Buenos Aires, Facultad de Ingeniería, Grupo de Medios Porosos, Paseo Colón 850, 1063, Buenos Aires, Argentina

ARTICLE INFO

Article history:
Received 4 August 2017
Received in revised form 2 October 2017
Accepted 15 November 2017
Available online 26 March 2018

Keywords:
Vibration
Incipient movement
Forced oscillator
3D DEM simulation

ABSTRACT

The onset of the movement of particles placed on a horizontal rough surface subject to a vertical sinusoidal vibration is investigated through tracking experiments, theoretical analysis, and numerical simulations. The frequency of vibration needed to move particles decays exponentially with the amplitude of the oscillatory input. This behavior is explained through a simple mechanism in which a forced damped harmonic oscillator with a spring constant represents all the interactions between the particle and the surface. The numerical results compare well with experimental data, demonstrating that the forces included in the numerical calculations suitably account for the main particle response, even though the complexity of the surface is not fully taken into account. Describing the way in which frequency varies with amplitude could be relevant to technological applications such as cleaning of material surfaces.

Introduction

The displacement of grains on surfaces in industrial processes frequently involves an external energy supply from disturbances in, for example, conveyor belts, truck transport, and drilling operations. As a result, the manipulation of granular matter always carries secondary effects, desired or not. Segregation, crushing, jamming, flow fluctuations, particle resuspension and saltation are just some examples. Much scientific attention is dedicated to the solution of the problems related to granular-material behavior, but many questions, especially those related to microscopic interactions between grains and surfaces, have not been answered.

The initiation of displacements of particles deposited on a surface has been shown to be crucial in predicting their possible further resuspension by air flow turbulence (Henry & Minier, 2014; Reeks & Hall, 2001; Valenzuela Aracena et al., 2017). The concept of "fluid threshold" (or the "aerodynamic threshold") was introduced by Bagnold many years ago (Bagnold, 1941; Chepil, 1945; Zingg, 1953). Moreover, the initial destabilization of sand grains by wind is important in resolving whether transport of sandy matter in deserts can be expected (Oger & Valance, 2017).

In the same way, vibration, as a perturbation of a particle's equilibrium, is relevant in many theoretical and applied problems, as, for instance, in the removal of small particles from surfaces in engineering applications (Ziskind, Fichman, & Gutfinger, 2000). Likewise, in manipulation stages of granular matter, the mechanical vibration of grains, either horizontal or vertical, is also an important external perturbation.

Naturally, if the vertical acceleration of vibration overcomes the gravitational acceleration, jumps are observed as typical movements of grains. Studies of the fluidization of granular beds subject to vibrations are common in the literature (Eshuis, van der Weele, van der Meer, Bos, & Lohse, 2007; Renard, Schwager, Pöschel, & Salueña, 2001; Mawatari, Koide, Tatemoto, Uchida, & Noda, 2002), in which the critical intensity required of the external excitations to fluidize grains has been reported. Moreover, even jamming of a drained granular medium was investigated showing its dependence on the time needed for grains to rearrange themselves (D'Anna & Gremaud, 2001). In recent years, the formation of patterns on the surface of vibrated layers of grains has been extensively studied. Depending on the whole set of parameters (such as amplitude and frequency of the excitation, shape and size of grains

* Corresponding author.
E-mail address: avidales@unsl.edu.ar (A.M. Vidales).

https://doi.org/10.1016/j.partic.2017.11.009

and container) different kinds of standing waves can be observed, with various textures (Melo, Umbanhowar, & Swinney, 1994, 1995; Metcalf, Knight, & Jaeger, 1997). Even basic studies concerning the excitation of small spheres deposited on a horizontal platform has been conducted in the past (Ripperger & Hein, 2005; Tippayawong & Preechawuttipong, 2011).

In describing a system consisting of a particle at rest on a vibrating surface, the first step is to consider a mechanical approach such as that presented in Dybwad (1985). There, the author studies the problem of a particle of mass m deposited on a vibrated surface (quartz resonator) as two coupled springs. The particle is linked to the surface via an elastic force with constant k. The quartz resonator has a mass M with an elastic constant K, and its resonance frequency depends only on its elastic properties. The frequency of the coupled system (particle–quartz resonator) is found to depend on the elastic force constant, k, of the particle. The frequency behavior is found to contradict the mass loading expectation, i.e., that the frequency of an oscillating system decreases when its mass increases. An experimental estimation of the value of the elastic constant shows that the actual area of contact of the two touching solids (particle and surface) is very much less than their geometrical area, i.e., than the area of contact that could be determined through a direct calculation, given that it may be lowered because of surface roughness (Dybwad, 1985).

As a second step in the description of the perturbation of a particle deposited on a surface, several linear and nonlinear oscillation models were introduced and analyzed in Ziskind et al. (2000) to demonstrate whether particle removal is possible for soft and hard particles on smooth and rough surfaces. One conclusion of that paper is that the natural frequency may be reduced by up to two orders of magnitude if the distance between two contacts at which the particle touches the surface is much smaller than the particle radius. Moreover, they emphasize the idea that the particle behavior is as if they were linked to the surface by springs (Dabros, Warszynsky, & van de Ven, 1994; Ziskind et al., 2000).

Experiments using aerosol particles deposited on a vibrating glass surface demonstrate that the wall vibration plays two opposing roles, i.e., to increase the separation force between particles and the wall, and to increase the particle deposition rate because of the active capture of aerosol particles (Theerachaisupakij, Matsusaka, Kataoka, & Masuda, 2002). In the same way, analytical models show that the frequency of the particle–surface interaction is found to significantly influence the removal rate of micro-particles from a vibrating surface (Tippayawong & Preechawuttipong, 2011). Furthermore, the description of re-entrainment requires the analysis of adhesion and capillary forces between particle and surface, the inertia of the particle when accelerated, and its contact interaction with particles resting on the surface, especially if the roughness is of order of the size of the beads deposited on it. For that reason, vibrating surfaces as an indirect means for the measurement of adhesion forces between a particle and a wall were used in Hein, Hucke, Stintz, and Ripperger (2002), by correlating particle re-entrainment events with the acting acceleration.

To conclude, we may say that the dynamics involved in the initiation of a particle movement on a surface subject to an external perturbation is not simple, and the inclusion of all parameters playing a role is not straightforward (Mullins, Michaels, Menon, Locke, & Ranade, 1992), even when only a threshold velocity for the initiation of movement is sought (Soepyan et al., 2016). As a result, the conditions under which the incipient motion of grains subject to vibration occurs remain unresolved, even for particles of millimeter size.

The aim of the present study is to predict the critical conditions for a particle to move when initially at rest on a vibrating surface, and to evaluate the physical parameters involved in this process. To pursue this objective, we performed a series of experiments using where particles (grains) of various sizes (within millimeter range) deposited on surfaces of different roughness values (built with micrometer glass beads) subject to a vibrational disturbance. We also develop a theoretical approach that describes the main aspects of the particle behavior found. The idea is to find the critical frequency–amplitude pairs needed to initiate the movement of the deposited grains for different bead sizes and materials and to demonstrate that the system behaves like a forced damped oscillator with a weak elastic constant (compared with that of the particle's material) given by the force interaction between particle and surface. In this sense, we follow the ideas previously developed in the work of Dybwad (1985) and Ziskind et al. (2000).

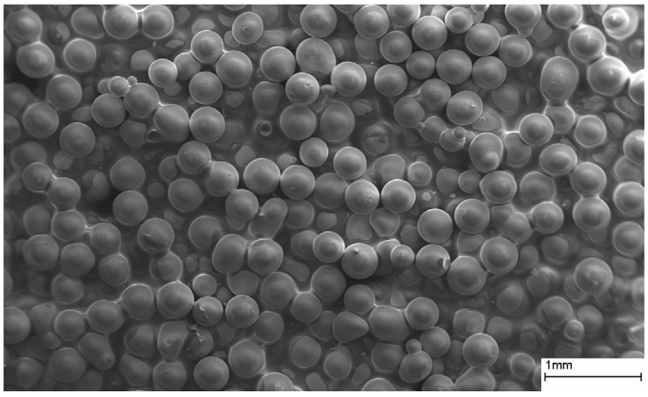

Fig. 1. SEM image of the surface composed of 250-μm-diameter glass beads.

To reinforce our goal, we also perform some numerical tests using a discrete element method with the appropriate interactions between grains and surface, to model the experimental conditions (Herrmann & Luding, 1998). Indeed, we reproduce well the set of experimental results when we included the elastic forces generated by the bead material and also those arising from adhesion and capillary effects.

Experiments

Experimental setup and materials

The apparatus used in the experiments consists of a horizontal rough surface, which vibrates vertically with a sinusoidal motion. Beads are placed on the surface to study the onset of their movement once the vibration begins. The rough surface is fabricated by gluing glass beads onto a flat circular plate of 6 cm in diameter. We worked with two different rough surfaces: one made with 250-μm glass beads and the other made of 500-μm glass beads, with respective size dispersions of 44 and 85 μm. A scanning electron microscope (SEM) image (Fig. 1) was taken to view directly the surface topography created by the 250-μm-diameter glued beads. Because of the way the surface was manufactured, some regions show surface pitting of the second or third layer of beads. This is also observed in the 500-μm-diameter beaded surface.

Regarding the free particles deposited on the surface, we used glass beads with mean diameters of (0.93 ± 0.02), (1.98 ± 0.04), (3.26 ± 0.09), and (3.98 ± 0.03) mm; and stainless-steel bearing balls of 2, 3, and 4 mm.

The plate is fixed to the drive arm of a mechanical oscillator and can vibrate with a selected frequency given by a wave generator connected to it. The plate subsequently induces a vibrational state of the rough surface. The amplitude of the oscillation of this arm is proportional to the signal (measured in volts) of the wave generator. The linear correspondence between voltage and amplitude is verified and calibrated carefully. To this end, we employed two different techniques. The one consists in tracing, with the help of

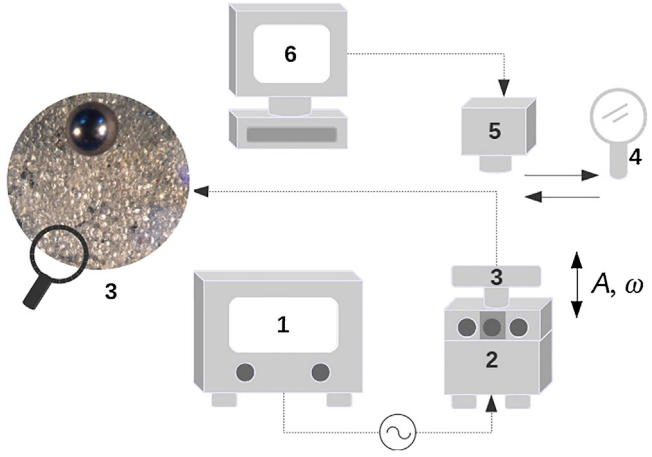

Fig. 2. Schematic of the experimental set-up used to measure the critical frequency–amplitude pairs: (1) sine wave generator, (2) mechanical wave driver, (3) rough surface, (4) loupe, (5) digital camera, and (6) computer.

a fine fiber pen, the trajectory of the oscillating arm-plate system. The double check is achieved by recording the movement of the arm-plate system with a video camera (EXILIM EX-ZR400, Casio, Japan). Fig. 2 gives a schematic of the experimental setup.

We also verified the dependence of the amplitude given by the generator in different frequency ranges and that the sinusoidal shape of the signal does not change with time. For the range involved in the present experiments, a constant amplitude can be provided that is independent of working frequency. Another important point is to know whether the critical frequency depends on the rate of increment during the experimental run. Indeed, we detected a dependence on the frequency rate, so a controlled ramp with a fixed rate equal to 0.63 rad/s^2 is used in all experiments.

In the present experiments we used sinusoidal waves with a given well-controlled amplitude, A, and frequency, ω. The values selected and measured for the amplitudes used in the experiments are: 0.73, 1.28, 1.91, 2.28, 2.58, 2.87, 3.12, 3.47, 3.88, and 4.03 mm, with an error of ±0.06 mm. The error in the different frequencies provided by the generator is of order 1 rad/s.

Initially, ten spheres with a given diameter were deposited randomly over the surface. They are carefully dispensed to prevent possible contact or collision among them or with the lateral edges, which are transparent thin walls stuck to the disk to avoid free particles from flowing out.

The desired amplitude is selected and fixed by the wave generator (Fig. 2) and the platform is subject to oscillations starting from a frequency of 0.10 Hz (approximately 0.63 rad/s) and increased in fixed steps at a rate of 0.10 Hz/s.

With the help of a magnifying glass, we checked for incipient movement of the particles and recorded the critical frequency, ω_c, at which at least half of the deposited spheres start to move from their original positions. Movement is considered when a particle has a displacement of the order of its radius. This behavior is also recorded by the digital video camera at 140 fps, to complete the determination of ω_c (Fig. 2). Once the critical frequency is reached, the experimental run ends, and the oscillator is turned off.

A new value for the amplitude of oscillation is chosen and the spheres are redistributed over the surface. The frequency is set to 0.10 Hz and the excitation is started again with the same increasing rate. The critical frequency for the new amplitude value is determined in the same way as explained above. To avoid important humidity effects, the experiments were always performed with a relative ambient humidity between 35% and 55%. This ensures the capillary interaction between the spheres and the surface is the same (Kohonena, Geromichalos, Scheel, Schier, & Herminghaus, 2004; Rabinovich et al., 2002). Finally, for a given surface and a given deposited sphere size and material, a set of 200 different positions on the surface are inspected to provide an average of results.

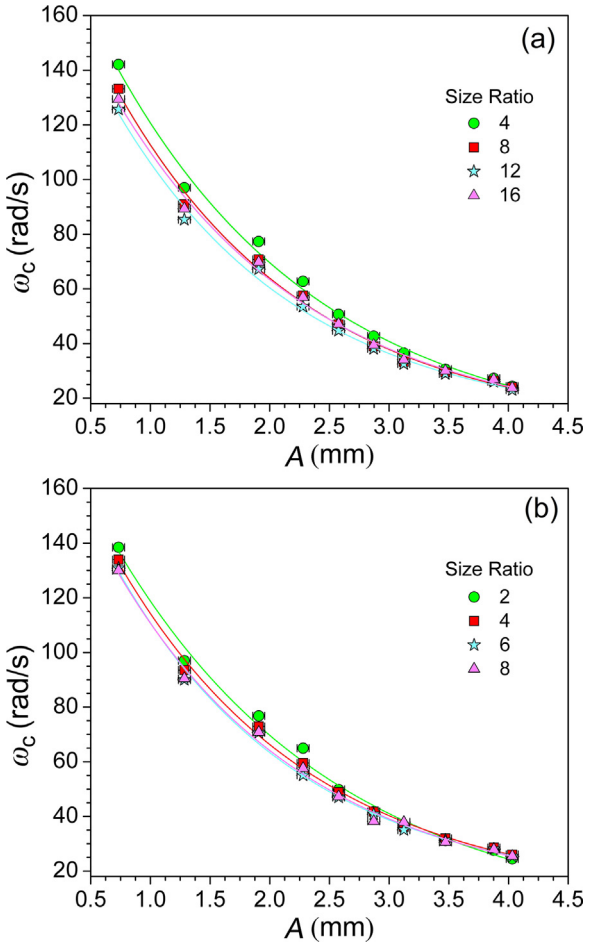

Fig. 3. Critical frequency as a function of the vibration amplitude for glass beads on (a) 250-μm and (b) 500-μm glass surface. The size ratios indicated correspond to the ratio between the diameter of the free spheres and the diameter of the beads comprising the surface. The error bars are indicated. The curves correspond to exponential fits.

Results and discussion

In our experiments, we observed that the positions of the beads that had moved were randomly distributed on the surface. In Fig. 3, we show the results obtained for the critical frequencies, ω_c, as the amplitude of the excitation is increased. The error bars for the amplitude are indicated and those for the statistical error in the determination of the critical frequency are of the order of the symbol size of the data point. Panels (a) and (b) correspond to the 250-μm and 500-μm beaded surfaces, respectively. The different ratios between the size of the free spheres and the size of the beads belonging to the surface are indicated in each case.

Furthermore, our results demonstrate the near independence of the size of the beads used in creating the rough surface. This implies that the surface roughness is such that its characteristic length is not governed by the size of the constituting beads, but rather by their geometrical arrangement formed with the glue. In other words, the topography of the surface created by the glued grains masks the influence of bead size.

Given the definition of ω_c, the set of points divides the upper region corresponding to the presence of movement of at least 50%

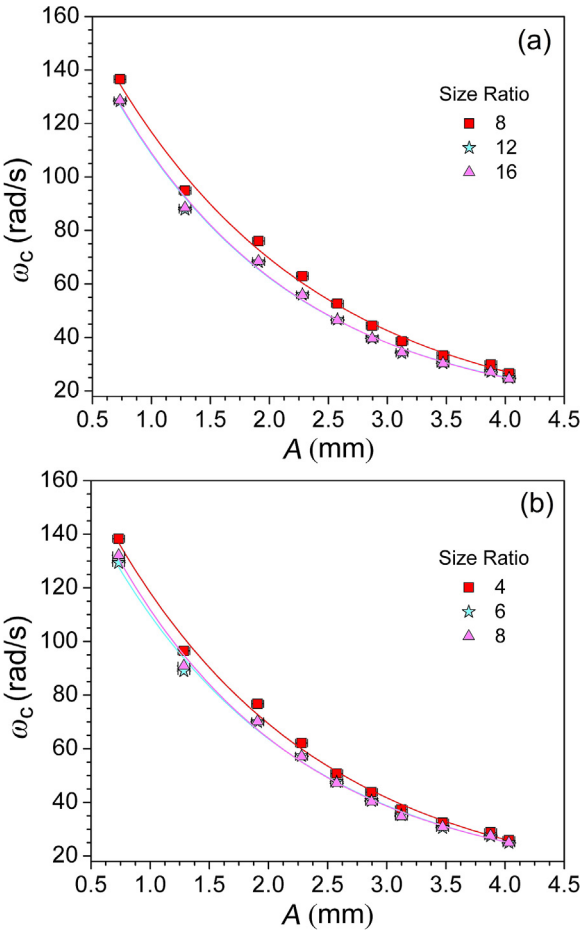

Fig. 4. As for Fig. 3 but for stainless steel spheres.

of the spheres from the lower part with absence of movement or with incipient movement of less than 50% of the particles.

The results for both surfaces and all ratios are quite similar. They can be fitted by an exponential decay function in all cases, independent of size ratio. Hence, as the amplitude of the oscillation increases, the critical frequency needed to initiate particle movement decreases.

To establish whether the behavior is still the same for different materials, we perform a series of experiments with stainless steel-spheres deposited on the same two rough surfaces. By following the same procedure outlined earlier, we obtained and plotted the results (Fig. 4). Comparing the two panels, it is clear that the behavior for both surfaces is practically the same, with a slight displacement of the data to higher frequencies for the smaller spheres. As indicated by the curves, the behavior can also be fitted by an exponential decay functions. Note that experiments with smaller 1-mm stainless-steel spheres were not performed to mitigate static charge effects.

From the results shown so far, a clear dependence on the excitation amplitude is experimentally seen in the critical frequency needed for a given particle to start its motion. In the regime where the system behaves as a lightly damped forced oscillator, it is expected that one natural resonance frequency is present. Nevertheless, the exponential decay of the critical frequency as the amplitude of vibration increases is very strong, as we shall see in the next section. The simple regime of a forced oscillator has to be rethought to explain our present results (Ziskind et al., 2000).

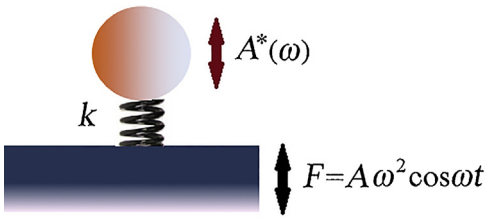

Fig. 5. Schematic of the forced damped harmonic oscillator representing our model system.

Theoretical approach

Modeling the results

We next explain from a theoretical point of view the possible physical mechanism yielding the experimental results presented above. Using a basic approach, we analyzed the situation of a free spherical particle on top of a vibrating bed. This system can be represented as a forced damped harmonic oscillator (Fig. 5).

We assume our system behaves like a harmonically excited oscillator with a spring representing the effective interactions between particle and surface. These interactions arise from intermolecular forces and capillary forces, which act when combined like an elastic bond ("spring") between the particle and surface with stiffness constant k (Ziskind et al., 2000). In this way, the stiffness constant represents the effective bond seen by the excited particles. Here, it is important to clarify that the attractive component of the effective interaction force in our model could be attributed to the presence of van der Waals and capillary effects. Indeed, these forces are still important when compared with gravitational forces, even for particles with sizes of a few millimeters. Both forces increase with particle radius, and it has been calculated that their values are not negligible with respect to particle weight (Israelachvili, 1991; Zhu, Zhou, Yang, & Yu, 2007). Although the relative humidity values at which experiments are performed is not very high, it suffices to generate capillary bridges between particles and surface requiring capillary forces to be considered in the problem (Herminghaus, 2005). In contrast, if these forces were not present, the sole inertial force resulting from the external excitation would yield a constant critical acceleration, which is not the case as will be shown below.

As discussed in Ziskind et al. (2000), the oscillatory motion of a particle on a surface is caused by the mechanical vibrations and the nonlinear effects that arise. The fact that the oscillation of a rough surface can generate a complex dynamic movement of the particle deposited on it compels considering nonlinear behavior. For a forced oscillator with a nonlinear force of restitution (Pain, 1976), depending on the sign of the nonlinear term, the effective spring constant was found to diminish with increasing spring deformation. We implemented this response in our model below.

It is very difficult to measure the elastic properties of the bond between particles and surface; nevertheless, the plotted experimental results (presented below) exhibited nonlinear behavior. Given the complexity of resolving the equations of motion with such behavior (Wang, 1999), we introduced an approximation by considering a simple linear damped harmonic oscillator with a correction for the dependence of the natural frequency on the oscillation amplitude (Ziskind et al., 2000).

We assume an external harmonic force is exerted via the spring on the particle by the vibrating bed. The vibration has amplitude A and frequency $\omega/2\pi$. Using standard oscillation analysis (see also Fig. 5), we calculated the magnitude of the force that the particle sees when the external excitation is applied. Following the theoretical model proposed here, one only has to recall the main

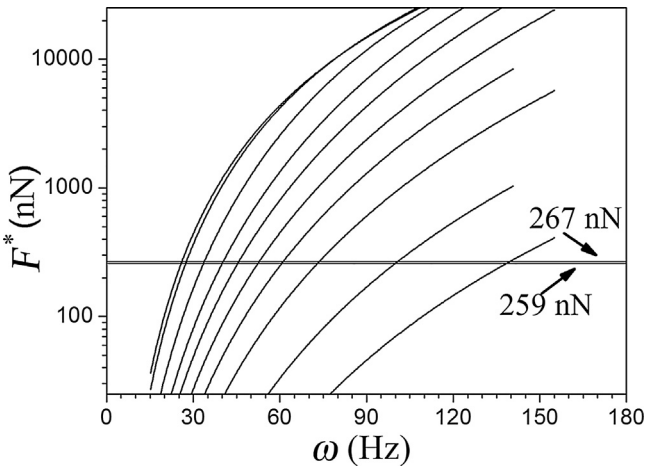

Fig. 6. Calculated forces experienced by the particle deposited on the oscillating surface for different amplitudes, which (from left to right) are: 0.73, 1.28, 1.91, 2.28, 2.58, 2.87, 3.12, 3.47, 3.88, 4.03 mm. Note that the force is plotted on a logarithmic scale. The two horizontal lines correspond to the detaching forces for each glass-beaded surface: 250 μm (upper) and 500 μm (lower).

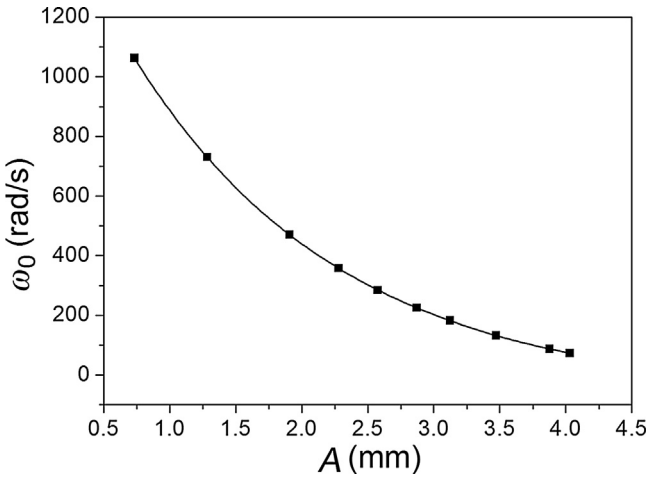

Fig. 7. Exponential decay assumption for the dependence of the natural frequency, ω_0, with the amplitude, A. The points correspond to values used in the theoretical calculations for both types of surfaces.

features concerning forced damped harmonic oscillations. Indeed, the amplitude is

$$A^*(\omega) = \frac{F_0/m}{\sqrt{\left(\omega_0^2 - \omega^2\right)^2 + (\gamma\omega)^2}}, \tag{1}$$

where ω_0 and γ are, respectively, the natural frequency of the system and the damping constant for the elastic bond between particle and surface. As is known, ω_0 depends on the stiffness of the bond. In the present case, experiments were performed by varying the frequency of the external excitation, so the amplitude of the force, F_0, is not a constant but varies with $A\omega^2$ (A the input amplitude of the oscillator), fixed for each experimental run. Thus, as the runs proceed, the amplitude seen by the sphere is

$$A^*(\omega) = \frac{A\omega^2}{\sqrt{\left(\omega_0^2 - \omega^2\right)^2 + (\gamma\omega)^2}}. \tag{2}$$

With this equation, the acceleration experienced by the particle is then $A^*(\omega)\omega^2$. When a different value for the amplitude A is chosen (a new experimental run begins by increasing the frequency) a new series of $A^*(\omega)$ values are seen by the particle as the experiment proceeds; as a consequence, the particle's velocity and acceleration change.

To illustrate our point, we apply the theoretical model to two of the experiments performed above. We consider glass spheres of 1 mm deposited on both the 250-μm and 500-μm glass-beaded surfaces. Fig. 6 shows the forces exerted on the particle deposited on the oscillating surface for each value of the amplitude, calculated using $F^* = mA^*(\omega)\omega^2$. Note that in our present model, the curves are the same for both types of surfaces. The mass of the sphere is 1.053×10^{-6} kg, obtained using 2500 kg/m^3 as the glass density. To better visualize the behavior, we plotted the results on a semi-log scale. The meaning of the two close horizontal lines is explained below. The ten curves correspond to different amplitudes of excitation used in the experiments, enumerated in the legend. A damping constant of 200 s^{-1} is adopted, which is (as seen below) of the order of the natural frequencies entering Eq. (2), thus modeling a lightly damped harmonic oscillator. In our checks, the results of the model appear almost independent of the value of this constant starting from 100 s^{-1} and one order of magnitude beyond. Only the range of oscillation frequencies involved in our experiments is displayed in the plots.

While some authors find that the stiffness of a spherical particle is not constant but increases with particle deformation (Ziskind et al., 2000), it is not unreasonable to believe that in our present scenario that k depends on the amplitude of the oscillation. In general, quantifying the elastic properties of the bond between particle and surface is difficult and hence some assumptions and estimations are done for the values of ω_0 used in the figures.

In our present case, it is expected that particle deformation becomes larger as the applied acceleration increases and, following Ziskind et al. (2000), stiffness constant k increases. Experimentally, the critical acceleration decreases as the input amplitude A increases (see below). Consequently, k decreases for increasing values of A. Given that the mass of the particles is constant, a decrease in k means a decrease in the natural frequency ω_0 of the system. With the exponential decay evident among the critical frequency–amplitude pairs found in our experiments, we propose, as a reasonable trend, an exponential decay of the natural frequency with amplitude A. This idea is consonant with the expected decay trend of the vibrating frequencies as the restoring force becomes non-linear (Kovacic, 2011).

Considering the range of values obtained for the experimental critical frequencies and their relationship with the different input amplitudes, we propose that the natural frequencies ω_0 obey a decay law with A, as displayed in Fig. 7. Note that these are the ω_0 values used to plot the curves in Fig. 6.

Now, consider the force necessary to overcome the interaction forces holding a particle attached to the surface (spring breaking). The horizontal lines in Fig. 6 represent this force, assuming that its value is constant for a given particle size. Although we do not know its precise value, its magnitude is of the order of nano-Newtons for micrometric particles on flat surfaces (Ripperger & Hein, 2005). Again, taking into account the range of values for ω_c found in our experiments, we are only able to estimate detaching forces of 267 nN and 259 nN for the 250-μm and 500-μm-bead surfaces, respectively. This rough estimation seems reasonable given that we are dealing with 1-mm-diameter particles on surfaces where attaching forces are expected to decrease because of surface roughness. We will discuss these values in the next section below.

The successive intersections of the horizontal lines with the different curves in Fig. 6 give the critical frequencies at which incipient movement of the particles is expected at a given amplitude of excitation. The values obtained at the intersections are plotted in Fig. 8, along with the corresponding experimental results evaluated from the data in Fig. 3(a) and (b). The agreement is quite good.

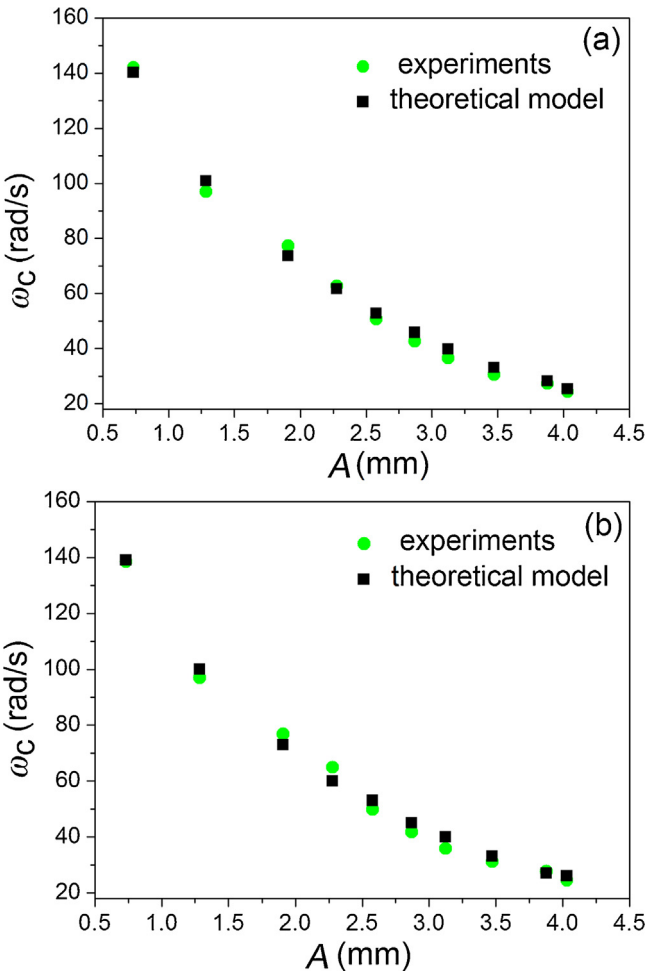

Fig. 8. Comparison between the experimental and theoretical values for the critical frequency–amplitude pairs for incipient movement of a 1-mm glass sphere over a: (a) 250-μm and (b) 500-μm glass-beaded surface.

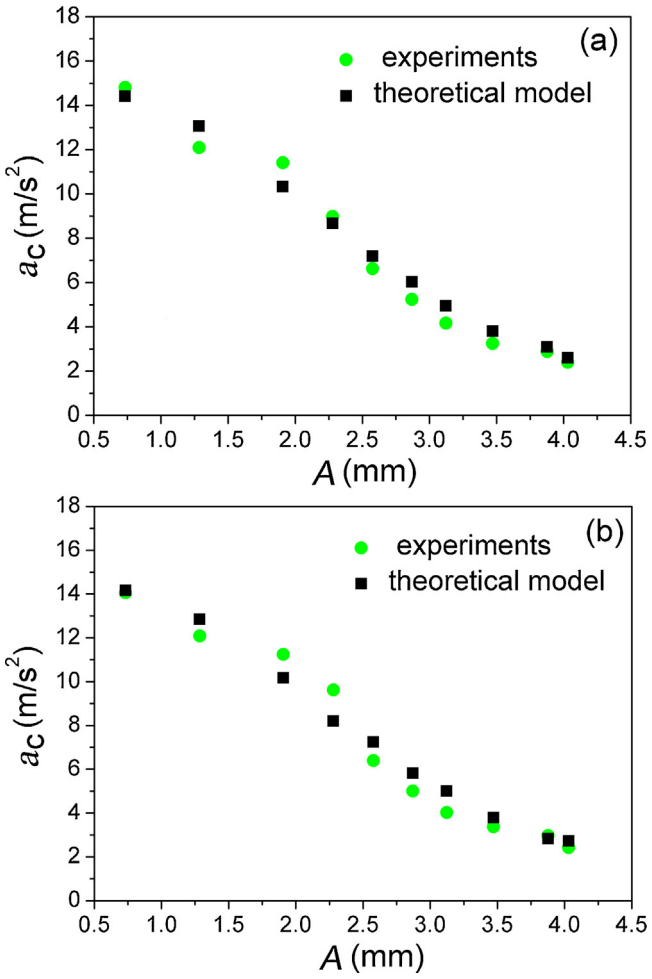

Fig. 9. Comparison between the experimental and theoretical values for the maximum critical acceleration the vibrating plate is subject to when particle movement begins for a 1-mm glass sphere resting on a (a) 250-μm and (b) 500-μm glass-beaded surface.

In the same way, taking the different values for ω_c obtained from the intersections, one can calculate as a function of amplitude the maximum critical acceleration, $a_c = A\omega_c^2$, the vibrating plate is subject to when 50% of the particle have moved. The results are presented for both surfaces in Fig. 9, along with experimental data. Here again, the agreement is good supporting the above-mentioned decreasing trend in ω_0 with amplitude.

Discussion

The theoretical approach developed here enables plots to be drawn of the force seen by the moving spheres as the external frequency increases, for different amplitudes. Given that in all cases, the moving particle is the same, the calculation of forces for both rough surfaces yields similar curves (Fig. 6). In contrast, the cohesion force (adhesion plus eventual capillary bridges) experienced by the particles when they try to detach from the surface (spring breaking) is different. The two values proposed (267 and 259 nN) for each case are very close reflecting the similar behavior found when comparing Fig. 3(a) and (b). They are derived by drawing the horizontal lines in Fig. 6 taking into account the experimental range of values within which ω_c varies with A. In other words, by noting the frequency range, the intersections of the horizontal line with each amplitude curve give the correct values of the experimental critical frequencies. Nevertheless, these force values from Fig. 6 are just rough estimates obtained from the model. Representing the force needed to destabilize the particle, they fall within the wide range of adhesion force estimates found in the literature (Zhu et al., 2007; Ripperger & Hein, 2005; Jones, Pollock, Cleaver, & Hodges, 2002). Evidently, if one could measure those forces, the reverse procedure predicts the critical frequency–amplitude range originally measured in our experiments.

In this way, one can conclude that the interaction of the spheres with both surfaces is quite similar and this is likely because of the way the surfaces were constructed. The high degree of disorder present in the spatial distribution of the glued beads on the surface is more important that their size, and therefore, the moving particles interact in a similar way with both surfaces.

Interestingly, in experiments with ideally rigid particles on a rigid plane undergoing sinusoidal vibration, the so-called Froude criterion is suitable to characterize critical detachment frequencies when only inertial forces are present. As stated above, adhesion forces must be included. For that reason, the experimental data cannot be represented by Froude criterion and one would have to modify that criterion to embody both the elastic and adhesion properties of the particle–plate system (Eshuis et al., 2007; Renard et al., 2001).

The model is able to describe quite well the experimental dependence of the critical frequencies on the input amplitude. Nevertheless, in consonance with Dabros et al. (1994) and Ziskind et al. (2000), the idea of a harmonic oscillator resonating at the natural frequency corresponding to the particle material is not adequate.

Although the exponential decrease in the critical frequency ω_c with amplitude A is not explicitly derived from theory, it can be appropriately deduced using the present model once an appropriate fitting of the spring stiffness ω_0 is implemented.

Finally, the decrease in acceleration as A increases is indicative of non-linear behavior in the natural frequency of the system. Indeed, assuming a dependence of ω_o on amplitude (Fig. 7) as with our simplified model is necessary to explain the results obtained experimentally.

Simulation model

We now present an outline of our simulation model to evaluate which are the main forces contributing to a good description of the problem and confirm that the inclusion of the elastic, adhesion, and capillary forces suffice to explain, from a numerical approach, the experimental behavior found.

Numerical setup

We use a classical discrete element method (DEM) model to represent the dynamical interaction between the moving particles and the rough surface. The present model follows the two-dimensional formulation of Savage (1993) and the three-dimensional extension used by Oger, Ippolito, and Vidales (2007). To unclutter the exposition, all equations are grouped in Appendix A.

The particles are modeled as spheres using a "soft-particle" approach (Eqs. (A1)–(A3)), where each sphere can have multiple contacts that may persist for extended contact durations (typically during 50 time steps). Normal and tangential forces can develop at the contact point between two spheres. When only compressive forces are allowed, the simulations represent dry, non-cohesive particle assemblies. The presence of tensile forces at the contacts models cohesive particles. In this case, short-range interactions occur up to the breaking of the adhesive forces or the severing of the liquid bridge. No long-range interactions are present in this model. In this way, bonds between contacting spheres can be introduced at the initial stage of the packing or during oscillations, thus mimicking an assembly of particles with tensile strengths.

In our model, a tensile (negative) value is possible up to a threshold tensile strength defined for the bond, after which the bond breaks. These bonds can arise, as expected, with the presence of van der Waals and/or capillary forces (Eqs. (A5) and (A4)). When no cohesive forces are present, contact takes place only when two spheres overlap, and the normal and tangential forces increase as the centers of the particles approach each other. The tangential force has also a critical tensile strength below which it is viscoelastic; above it, the bond breaks and the tangential force follows the Mohr–Coulomb law.

To simulate local contact effects and non-perfect spherical particles, a rolling resistance parameter has been introduced recently (Ai, Chen, Rotter, & Ooi, 2011). This parameter represents the effects of the shape of the particle on its rolling capability and the possible resistance because of plastic deformation during contact and/or possible viscous hysteresis. We consider this parameter in our model and its value is taken between the range 0 (no effect) to 0.4, which is the maximum value that the slope angle can attain when the rolling-resistance torque equals that produced by gravity acting on the particle.

To simulate the experimental setup, we first configured a rough surface of glued spheres with diameter 500 μm. We randomly deposited up to three layers of these spheres on the surface. In all cases, the spheres are stable under gravity with one contact for the first layer, and up to three contacts for the two upper layers. Thereafter, all the spheres are assumed as fixed in their positions and motionless with respect to the vibrating plate. They only interact with the upper moving spheres. This glued layer simplifies the global interaction calculation, as only sphere contacts are present in the simulation, i.e., no flat wall-sphere interactions are possible.

Table 1
Input parameters for the 500-μm glass-beaded surface and 1-mm moving glass beads at 70% of relative humidity.

Parameter	Value
Density for glass (kg/m^3)	2500
Coefficient of friction, μ_i	0.5
Coefficient of restitution	0.8
Stiffness, K_n (N/m)	10^6
Stiffness, K_t (N/m)	1.6×10^6
Dashpot constant, b_n (kg/s)	0.11
Dashpot constant, b_t (kg/s)	$0.4b_n$
Rolling resistance coefficient	0.3
Surface tension, γ_{sl} (mN/m)	72
Hamaker coefficient, A_H (J)	6.5×10^{-20}

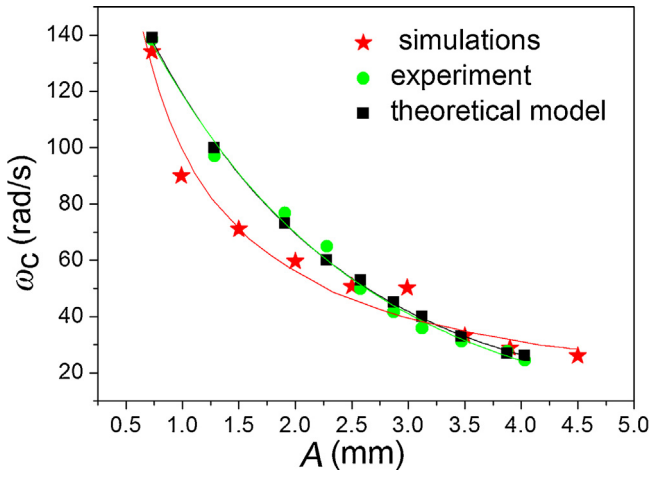

Fig. 10. Comparison of simulation results with experimental and theoretical results for critical frequency–amplitude pairs for a surface of 500-μm glass beads and 1-mm moving particles.

Once the rough surface is ready, 200 spheres of 1-mm diameter are randomly deposited on it to consider a large number of different configurations. To speed up the computation, we prevent contacts between particles, i.e., no billiard-ball effects are present during simulations. Once the moving spheres attain equilibrium positions, the surface constituted by the glued spheres is vertically oscillated with a given amplitude and frequency by moving the center of each sphere. In the presence of interaction forces, this process consequently oscillates all spheres. Note that this oscillation limits the choice of time step for simulations. Indeed, apart from the classical soft DEM rule, for which the length of the time step for numerical integration is 1/50 of the duration of the collisions, we have to take into account that the displacement associated with the oscillation of the glued spheres generates an overlap with the upper spheres that must also follow the soft DEM rule.

Since increasing the frequency step by step, as in experiments, is computationally time consuming, we ran the program a few times for each frequency–amplitude pair and looked for spheres that has moved after a given time. Thus, we can easily achieve the 50% threshold of moving spheres with good statistics. The set of input parameters used in the simulation are given in Table 1.

Results and discussion

In Fig. 10, we show the simulation results for the critical frequency–amplitude pair for the 500-μm glass-beaded surface

and glass beads with diameter 1 mm. The corresponding experimental and theoretical results are shown for comparison. The exponential decay is recovered again in simulations and the agreement with experiments is reasonably good. The lines in the figure indicate fitted exponential curves.

We understand that the main reason for the difference in behavior between simulations and experiments is surface roughness. In simulations, the number of layers and the mean distance between spheres in these upper layers do not have the topological complexity of the surface generated through real glued spheres. In this way, the ease with which the moving beads overcome the barrier from a hole is greater in simulations than for experiments. This is evident especially for lower amplitudes where the critical frequencies observed in simulations are lower. We also tried other ratios and confirmed this behavior. This will be the subject of further research.

Conclusions

In this work, we determined experimentally the critical moment when particles deposited on a vibrating surface are set in motion. Although the experimental setup is rather simple, the explanation of the exponential decay relationship found for the critical frequency–amplitude pairs is not straightforward. As discussed in previous work (Ziskind et al., 2000), our experiments show that the frequencies are much lower than those related to the elastic properties of particle material (6×10^6 rad/s or higher). These frequencies follow an exponential decay with the amplitude of the external sinusoidal excitation.

Following up the idea that particles behave like a forced damped oscillator, we developed a simple resonant spring model based on the assumption that the stiffness of the vibrating spring accounts for all the moving particle interactions with the surface and results in a lower value than that with just the stiffness of glass alone. Moreover, it is necessary to assume that the natural frequency of the spring depends on particle deformation and, as a consequence, on the acceleration amplitude of vibration. This is in line with other authors' arguments, for which the stiffness constant of oscillators depends on the external excitation for both linear and non-linear restoring forces (Ziskind et al., 2000; Kovacic, 2011). The idea of a harmonic oscillator resonating at a natural frequency corresponding to the particle material, alone, is inadequate. In this way, the theoretical model proposed here describes the experimental behavior quite closely, explaining the exponential decay obtained for critical frequencies, although it is not explicitly derived from theory.

Contrary to the theoretical model, where the elastic constant can be thought of as the result of all interactions of the particle with the surface, in the simulation model, the lack of a real topological description of surface roughness is responsible for the lower-than-expected result for the critical frequencies result, especially for lower amplitudes given that space barriers are more difficult for moving particles to overcome. In this sense, a deeper study of the critical frequency–amplitude pairs for incipient movement of particles on a highly controlled monolayer of glued spheres remains an open problem.

Acknowledgments

We acknowledge financial support from Universidad Nacional de San Luis through PROICO 310114, from CONICET through PIP 353, from MYNCyT-ECOS Sud, Argentine-France, project A15E03 and LIA CONICET-CNRS Physique et Mécanique de Fluides.

Appendix A.

Spring-dashpot model for particle contact

The i-th particle is characterized by its radius $\boldsymbol{r}_i$, the position of its center (x_i, y_i), and the angular rotation θ_i around its center. Interparticle forces exist only when two spheres overlap or when the cohesive forces keep them in close contact, and the normal and tangential contact forces increase as the centers of the particles approach each other.

The normal force F_n at the contact is modeled as viscoelastic. It consists of an elastic (a linear spring) and a viscous damping (a linear dashpot) contributions, described as follows:

$$\begin{aligned} &\text{Compression}: \quad F_\mathrm{n} = K_\mathrm{n}\delta - b_\mathrm{n}v_\mathrm{n} \quad \text{for} \quad \delta = \left(\sigma - |\boldsymbol{r}_i - \boldsymbol{r}_j|\right) > 0 \\ &\text{Tension}: \quad\quad F_\mathrm{n} = 0 \quad\quad\quad\quad\quad\quad\quad\quad \text{for} \quad \delta < 0 \end{aligned} \tag{A1}$$

where K_n is the spring constant for the normal forces, δ the relative normal displacement between the centers of the two particles in contact, σ the distance between their two centers, $\boldsymbol{r}_i$ and $\boldsymbol{r}_j$ are the two radii of the particles, v_n is the relative normal velocity, and b_n the dashpot constant for normal forces.

The force in the tangential direction is also modeled as viscoelastic with contributions from a linear spring and a linear dashpot,

$$F_\mathrm{t} = K_\mathrm{t}\delta_\mathrm{t} - b_\mathrm{t}v_\mathrm{t}, \tag{A2}$$

where K_t is the spring constant for tangential forces, δ_t the relative lateral displacement during contact, v_t the relative tangential velocity, and b_t the dashpot constant for tangential forces. F_t has a threshold value, a maximum that is chosen according to the Coulomb friction law where slipping can occur,

$$F_\mathrm{t} = \mu_\mathrm{i}F_\mathrm{n}, \tag{A3}$$

where μ_i is the coefficient of friction. The tangential force acts in a direction opposite to that of the relative tangential velocity v_t.

The definition of the two spring constants and the two dashpot terms can be directly related to the classical mechanical parameters describing a material, i.e., Young's modulus, Poisson's ratio, and coefficient of restitution (see, for example, Mishra and Murty (2001)).

In the present model, we can introduce bonds between spheres that are in contact depending on the surrounding water content. The decrease in cohesive force (F_cap) during the separation of the two adjacent spheres is modeled using the equation proposed by Charlaix and Crassous (2005),

$$F_\mathrm{cap} = 2\pi\gamma_\mathrm{sl}R\cos\left(\theta\right), \tag{A4}$$

where $\cos(\theta)$, defined from the wetting angle, is around 0.84 for water on glass, γ_sl is the liquid surface tension and R the effective radius of the two interacting particles.

Finally, the van der Waals force between particles, F_VW, is modeled through a solely attractive force as (Israelachvili, 1991)

$$F_\mathrm{VW} = \frac{A_\mathrm{H}R}{6D^2}, \tag{A5}$$

where A_H is the Hamaker coefficient, R the effective radius (as in Eq. (A4)), and D the distance between the surfaces.

References

Ai, J., Chen, J.-F., Rotter, J. M., & Ooi, J. Y. (2011). Assessment of rolling resistance models in discrete element simulations. *Powder Technology, 206*, 269–282.

Bagnold, R. A. (1941). *The physics of blown sand and desert dunes*. London: Chapman & Hall.

Charlaix, E., & Crassous, J. (2005). Adhesion forces between wetted solid surfaces. *The Journal of Chemical Physics, 122*, 184701.

Chepil, W. S. (1945). Dynamics of wind erosion: I. Nature of movement of soil by wind. *Soil Science, 60*, 305–320.

Dabros, T., Warszynsky, P., & van de Ven, T. G. N. (1994). Motion of latex spheres tethered to a surface. *Journal of Colloid Interface Science*, *162*, 254–256.
D'Anna, G., & Gremaud, G. (2001). Vibration-induced jamming transition in granular media. *Physical Review E*, *64*, 011306.
Dybwad, G. L. (1985). A sensitive new method for the determination of adhesive bonding between a particle and a substrate. *Journal of Applied Physics*, *58*, 2789–2790.
Eshuis, P., van der Weele, K., van der Meer, D., Bos, R., & Lohse, D. (2007). Phase diagram of vertically shaken granular matter. *Physics of Fluids*, *19*, 123301.
Herminghaus, S. (2005). Dynamics of wet granular matter. *Advances in Physics*, *54*, 221–261.
Hein, K., Hucke, T., Stintz, M., & Ripperger, S. (2002). Analysis of adhesion forces between particles and wall based on the vibration method. *Particle & Particle Systems Characterization*, *19*, 269–276.
Henry, C., & Minier, J.-P. (2014). Progress in particle resuspension from rough surfaces by turbulent flows. *Progress in Energy and Combustion Science*, *45*, 1–53.
Herrmann, H. J., & Luding, S. (1998). Modeling granular media on the computer. *Continuum Mechanics and Thermodynamics*, *10*, 189–231.
Israelachvili, J. N. (1991). *Intermolecular and surface forces*. London: Academic Press.
Jones, R., Pollock, H. M., Cleaver, J. A. S., & Hodges, C. S. (2002). Adhesion forces between glass and silicon surfaces in air studied by AFM: Effects of relative humidity, particle size, roughness and surface treatment. *Langmuir*, *18*, 8045–8055.
Kohonena, M., Geromichalos, D., Scheel, M., Schier, C., & Herminghaus, S. (2004). On capillary bridges in wet granular materials. *Physica A*, *339*, 7–15.
Kovacic, I. (2011). Forced vibrations of oscillators with a purely nonlinear power-form restoring force. *Journal of Sound and Vibration*, *330*, 4313–4327.
Luding, S. (1998). Collisions & contacts between two particles. In H. J. Herrmann, J.-P. Hovi, & S. Luding (Eds.), *Physics of dry granular media* (pp. 285–304). Amsterdam: Kluwer Academic Publishers. NATO ASI Series E350.
Mawatari, Y., Koide, T., Tatemoto, Y., Uchida, S., & Noda, K. (2002). Effect of particle diameter on fluidization under vibration. *Powder Technology*, *123*, 69–74.
Melo, F., Umbanhowar, P. B., & Swinney, H. L. (1994). Transition to parametric wave patterns in a vertically oscillated granular layer. *Physical Review Letters*, *72*, 172–175.
Melo, F., Umbanhowar, P. B., & Swinney, H. L. (1995). Hexagons, kinks, and disorder in oscillated granular layers. *Physical Review Letters*, *75*, 3838–3841.
Metcalf, T. H., Knight, J. B., & Jaeger, H. M. (1997). Standing wave patterns in shallow beds of vibrated granular material. *Physica A*, *236*, 202–210.
Mishra, B. K., & Murty, C. V. R. (2001). On the determination of contact parameters for realistic DEM simulations of ball mills. *Powder Technology*, *115*, 290–297.
Mullins, M. E., Michaels, L. P., Menon, V., Locke, B., & Ranade, M. B. (1992). Effect of geometry on particle adhesion. *Aerosol Science and Technology*, *17*, 105–118.
Oger, L., Ippolito, I., & Vidales, A. M. (2007). How disorder can diminish avalanche risks: Effect of size distribution. *Granular Matter*, *9*, 267–278.
Oger, L., & Valance, A. (2017). Model of the saltation transport by discrete element method coupled with wind interaction. *European Physical Journal Web of Conferences*, *140*, 12004.
Pain, H. J. (1976). *The physics of vibrations and waves* (2nd ed.). New York: John Wiley & Sons.
Rabinovich, Y. I., Adler, J., Esayanur, M. S., Ata, A., Singh, R., & Moudgi, B. (2002). Capillary forces between surfaces with nanoscale roughness. *Advances in Colloid and Interface Science*, *96*, 213–230.
Reeks, M. W., & Hall, D. (2001). Kinetic models for particle resuspension in turbulent flows: Theory and measurement. *Journal of Aerosol Science*, *32*, 1–31.
Renard, S., Schwager, T., Pöschel, T., & Salueña, C. (2001). Vertically shaken column of spheres. Onset of fluidization. *The European Physical Journal E*, *4*, 233–239.
Ripperger, S., & Hein, K. (2005). Measurement of adhesion forces in air with the vibration method. *China Particuology*, *3*, 3–9.
Savage, S. B. (1993). Disorder, diffusion, and structure formation in granular flows. In D. Bideau (Ed.), *Disorder and granular media* (p. 264). Amsterdam: North Holland.
Soepyan, F., Cremaschi, S., McLaury, B., Sarica, C., Subramani, H., Kouba, G., et al. (2016). Threshold velocity to initiate particle motion in horizontal and near-horizontal conduits. *Powder Technology*, *292*, 272–289.
Theerachaisupakij, W., Matsusaka, S., Kataoka, M., & Masuda, H. (2002). Effects of wall vibration on particle deposition and reentrainment in aerosol flow. *Advanced Powder Technology*, *13*, 287–300.
Tippayawong, N., & Preechawuttipong, I. (2011). Analysis of microparticle resuspension in turbulent flows with horizontally vibrating surface. *Australian Journal of Basic and Applied Sciences*, *5*, 356–363.
Valenzuela Aracena, K. A., Benito, J. G., Oger, L., Uñac, R. O., Ippolito, I., & Vidales, A. M. (2017). Experiments and numerical modeling for the movement and resuspension of grains. *European Physical Journal Web of Conferences*, *140*, 03014.
Wang, L. (1999). The role of damping in phase imaging in tapping mode atomic force microscopy. *Surface Science*, *429*, 178–185.
(1953). Wind tunnel studies of the movement of sedimentary material. *Proceedings of the 5th Hydraulic Conference Bulletin*, *Vol. 34*, 111–135.
Ziskind, G., Fichman, M., & Gutfinger, C. (2000). Particle behavior on surfaces subjected to external excitations. *Journal of Aerosol Science*, *31*, 703–719.
Zhu, H. P., Zhou, Z. Y., Yang, R. Y., & Yu, A. B. (2007). Discrete particle simulation of particulate systems: Theoretical developments. *Chemical Engineering Science*, *62*, 3378–3396.